Analytical and adaptive numerical evaluation of all terms required in a 3D boundary element implementations for potential problems using linear triangle elements

Ney Augusto Dumont[1], Tatiana Galvão Kurz[1]

[1]*Department of Civil and Environmental Engineering, Pontifical Catholic University of Rio de Janeiro*
Rua Marquês de São Vicente 225, 22451-900, Rio de Janeiro, Brazil
dumont@puc-rio.br, tatianagk.eng@gmail.com

Abstract. The present contribution introduces a formulation for 3D steady-state potential and elastostatics problems that ends up with the analytical handling of all integrals necessary in an implementation using linear triangle (T3) elements – whether regular, improper, quasi-singular, singular or hypersingular integrals are involved. The boundary element matrices – including the discontinuous term of the double-layer potential matrix – are obtained in a straightforward way with the use of analytically pre-evaluated integrals. Results at internal points that may be located arbitrarily close to the boundary are also given analytically. The paper describes the main concepts and computational features of the proposed formulation and presents an example of 3D potential problem to illustrate the most challenging topological configurations one might deal with in practical applications. For source points sufficiently far from a boundary element an adaptive numerical integration scheme is also proposed for the sake of computational speed – and how far a point should be in order to be considered far is also discussed.

Keywords: Collocation boundary element method, Numerical integration, Analytical integration, 3D Problems

1 Introduction

The collocation boundary element method (BEM) [1] has been recently reconceptualized by the first author for general 2D and 3D problems [2], who has also proposed a general, simple and unified procedure for the machine-precision treatment of all kinds of singularities that may occur in 2D steady-state potential and elastostatics problems [2].

The numeric issues for 3D problems are of a completely different nature [3, 4]. The triangle-to-square coordinate transformation for the evaluation of improper integrals in a computationally economical way seems to have been firstly suggested for BEM applications in [5]. More literature references to the theme are given in [3, 4].

Simple analytical results are obtained for all kinds of integrals required for 3D steady-state potential and elastostatics problems – for the boundary discretized with flat segments. This includes the evaluation of results at arbitrarily placed internal points, with hypersingularities also dealt with analytically. The case of a generally curved boundary segment is still not considered by the authors – and may not be mastered in the present framework. Although the proposed developments apply directly to elastostatics problems, space restrictions force us to draw attention only to potential problems.

2 Problem formulation

The following developments, as outlined in [3, 4], apply to the adequate evaluation of integrals that may either be improper or embed singularities or quasi-singularities. The source point 0 is indicated on the left in Fig. 1, where $r = \sqrt{(x-x_0)^2 + (y-y_0)^2 + (z-z_0)^2}$ is the distance from the singularity (0 or source) point $(x_0, y_0, z_0) \equiv (x(\xi_s, \eta_s),\ y(\xi_s, \eta_s),\ z(\xi_s, \eta_s))$ to a generic (F or field) point $(x, y, z) \equiv (x(\xi, \eta),\ y(\xi, \eta),\ z(\xi, \eta))$, both in Cartesian coordinates and in terms of the indicated natural triangle coordinates $(\xi \in [0, 1-\eta],\ \eta \in [0, 1])$.

The triangle to sub-triangles transformations outlined on the right in Fig. 1 are – to the authors' best knowledge – a novel generalization of a transformation classically proposed in the literature on finite and boundary element methods that uses a square-to-triangle degeneration in order to deal with a singularity [5]. Prior to pro-

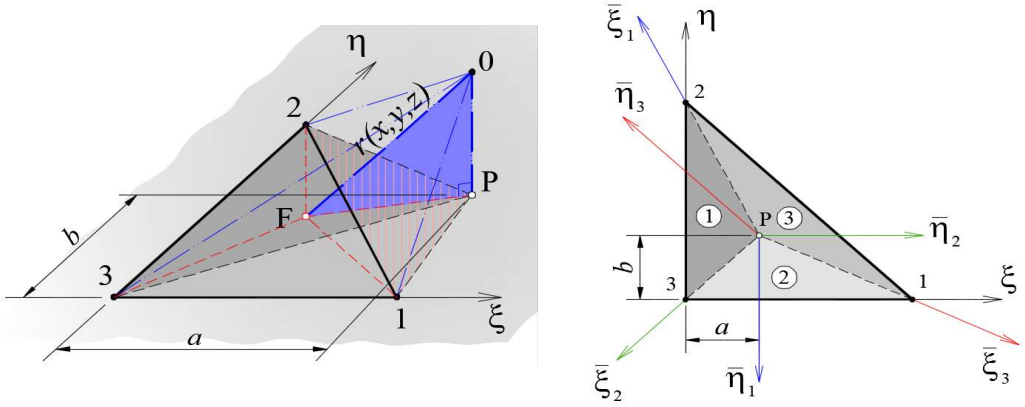

Figure 1. Representation of the quasi-singular source point 0 in the Cartesian space for a triangle element, and description with two different systems of natural coordinates, (ξ, η) and $(\tilde{\xi}_l, \tilde{\eta}_l)$ referred to the projection P of the source point onto the triangle's plane

moting an eventual singularity cancellation, the introduced coordinate transformation reshapes the integrals so as they become eventually evaluated using a symbolic tool kit. For an analytical function $f\,(\xi, \eta)$, integration is carried out over transformed spaces corresponding to the three indicated sub-triangles, $\widehat{\mathrm{P12}}$, $\widehat{\mathrm{P23}}$ and $\widehat{\mathrm{P31}}$,

$$\int_0^1 \int_0^{1-\eta} f\,(\xi,\eta)\,\mathrm{d}\xi\mathrm{d}\eta = \sum_{l=1}^{3} \int_0^1 \int_0^1 f\left(\xi(\tilde{\xi}_l,\tilde{\eta}_l),\eta(\tilde{\xi}_l,\tilde{\eta}_l)\right)\left|J_l(\tilde{\xi}_l,\tilde{\eta}_l)\right| \mathrm{d}\tilde{\xi}_l\mathrm{d}\tilde{\eta}_l, \tag{1}$$

considered as degenerated square subspaces $\left(\tilde{\xi}_l \in [0,1], \tilde{\eta}_l \in [0,1]\right)$, $l = 1,2,3$, where one of the nodal points of the unit square collapses in order to coincide with the point of singularity P($\xi = a, \eta = b$) – the projection of the source point onto the boundary element's plane. The auxiliary coordinate systems $(\tilde{\xi}_l, \tilde{\eta}_l)$ have origin at node P and are oriented as indicated. Depending on the depicted values of a and b one or two of these triangles may be void or correspond to negative areas, so that cases of real singularity and quasi-singularity are dealt seamlessly in the same algorithm. In the presently proposed general approach, the singularity point 0 may be located outside the (ξ, η) plane, as shown on the left in Fig. 1. The distance from the source 0 to a field point F on the element is the hypotenuse $\overline{\mathrm{0F}}$ of the right triangle whose legs are the distances $\overline{\mathrm{0P}}$ from the source point to the plane and $\overline{\mathrm{PF}}$.

According to this proposition, the coordinates (ξ, η) are linear transformations of $(\tilde{\xi}_l, \tilde{\eta}_l)$ [3, 4]:

$$[\xi,\eta]_1 = \left[a(1-\tilde{\xi}_1), \tilde{\xi}_1(1-b-\tilde{\eta}_1)+b\right]; \quad |J|_1 = \tilde{\xi}_1 a \quad \text{for sub-triangle } \Delta_1 \tag{2}$$

$$[\xi,\eta]_2 = \left[\tilde{\xi}_2(\tilde{\eta}_2-a)+a, b(1-\tilde{\xi}_2)\right]; \quad |J|_2 = \tilde{\xi}_2 b \quad \text{for sub-triangle } \Delta_2 \tag{3}$$

$$[\xi,\eta]_3 = \left[\tilde{\xi}_3(1-a-\tilde{\eta}_3)+a, \tilde{\xi}_3(\tilde{\eta}_3-b)+b\right]; \quad |J|_3 = \tilde{\xi}_3(1-a-b) \quad \text{for sub-triangle } \Delta_3. \tag{4}$$

The ratio $|J|_l / r(\tilde{\xi}_l, \tilde{\eta}_l)$ is always finite, which justifies the classically proposed coordinate transformation. However, the decisive advantage of this transformation for the present developments is the separation of terms of the variables $\tilde{\xi}_l$ and $\tilde{\eta}_l$, which enables the analytical evaluation of the problem's key integrals [3, 4]. In fact, the square distance $\Delta r^2 \equiv \overline{\mathrm{0F}}^2 = \overline{\mathrm{0P}}^2 + \overline{\mathrm{PF}}^2$ of Fig. 1) becomes expressed for each subtriangle as

$$\Delta r^2 = \Delta r_0^2 + c_l^2 \tilde{\xi}_l^2 \equiv \Delta r_0^2 + \left(\tilde{a}_l \tilde{\eta}_l^2 + \tilde{b}_l \tilde{\eta}_l + \tilde{c}_l - \Delta r_0^2\right)\tilde{\xi}_l^2 \equiv \Delta r_0^2 + c_l^2 \tilde{\xi}_l^2, \tag{5}$$

where $\Delta r_0^2 \equiv \overline{\mathrm{0P}}^2$. Since the triangle's area cannot be void and integration is carried out only for a sub-triangle of non-void area, following geometric properties are paramount in the analytical integral evaluations:

$$\tilde{a}_l > 0, \quad \tilde{c}_l > 0; \quad \tilde{a}_l \tilde{\eta}_l^2 + \tilde{b}_l \tilde{\eta}_l + \tilde{c}_l > 0; \quad 4\tilde{a}_l \tilde{c}_l - \tilde{b}_l^2 > 0. \tag{6}$$

All particularities of sub-triangles with void or negative areas (then, void or negative integrals) are taken into account by the Jacobian transformations given in eqns (2)-(4).

3 Evaluations for potential problems

Owing to space restrictions, the explicit expressions for the single- and double-layer potential matrices **G** and **H** for 3D potential and elasticity [1] are not given. The developments for arriving at such expressions are actually

relevant to show the kind of integrals we must deal with as well as how important it is to take the properties outlined above into account [3, 4]. All integrals could be evaluated analytically using the mathematical software Maple[1] and some ingenuity.

They are, schematically, for the single-layer potential matrix $\mathbf{G}$:

$$\int_0^1 \int_0^1 \frac{\left\langle 1 \quad \tilde{\xi}_l \quad \tilde{\xi}_l\tilde{\eta}_l \right\rangle}{\sqrt{\Delta r_0^2 + c_l^2\tilde{\xi}_l^2}} \tilde{\xi}_l \, \mathrm{d}\tilde{\xi}_l \mathrm{d}\tilde{\eta}_l, \quad l = 1,2,3 \quad \text{for } \Delta r_0^2 \geq 0, \tag{7}$$

and for the double-layer potential matrix $\mathbf{H}$ (integrals void for $\Delta r_0^2 = 0$):

$$\int_0^1 \int_0^1 \frac{\left\langle 1 \quad \tilde{\xi}_l \quad \tilde{\xi}_l\tilde{\eta}_l \right\rangle}{\left(\Delta r_0^2 + c_l^2\tilde{\xi}_l^2\right)^{3/2}} \tilde{\xi}_l \, \mathrm{d}\tilde{\xi}_l \mathrm{d}\tilde{\eta}_l, \quad l = 1,2,3; \quad \Delta r_0^2 > 0. \tag{8}$$

The above expressions are valid for potential results at internal points, as well. For gradient results, we have

$$\int_0^1 \int_0^1 \begin{bmatrix} 1 & \tilde{\xi}_l & \tilde{\xi}_l\tilde{\eta}_l \\ \cdot & \tilde{\xi}_l^2 & \tilde{\xi}_l^2\tilde{\eta}_l \\ \cdot & \cdot & \tilde{\xi}_l^2\tilde{\eta}_l^2 \end{bmatrix} \frac{\tilde{\xi}_l \, \mathrm{d}\tilde{\xi}_l}{\left(\Delta r_0^2 + c_l^2\tilde{\xi}_l^2\right)^{p/2}} \mathrm{d}\tilde{\eta}_l, \;\; p = 3 \text{ or } 5, \;\; l = 1,2,3; \;\; \Delta r_0^2 > 0 \tag{9}$$

$$\int \int \begin{bmatrix} 1 & \tilde{\eta}_l & \tilde{\eta}_l^2 \\ \cdot & 1/\tilde{\xi}_l & \tilde{\eta}_l/\tilde{\xi}_l \end{bmatrix} \frac{\mathrm{d}\tilde{\xi}_l}{c_l^3} \mathrm{d}\tilde{\eta}_l, \quad l = 1,2,3 \quad \text{for } \Delta r_0^2 = 0. \tag{10}$$

In the latter cases, when a singularity occurs due to $\tilde{\xi}$ in the denominator, the integration intervals become

$$\int_0^1 \int_0^{1-\eta} f \, \mathrm{d}\xi \mathrm{d}\eta =$$

$$\begin{cases} \left|\tilde{J}\right|_1 \int_0^1 \left(\int_{\frac{b}{b+\tilde{\eta}_1-1}}^1 \left(f\tilde{\xi}_1\right) \mathrm{d}\tilde{\xi}_1 \right) \mathrm{d}\tilde{\eta}_1 + \left|\tilde{J}\right|_3 \int_0^1 \left(\int_{\frac{b}{b-\tilde{\eta}_3}}^1 \left(f\tilde{\xi}_3\right) \mathrm{d}\tilde{\xi}_3 \right) \mathrm{d}\tilde{\eta}_3 & \text{for} \quad b < 0 \\ \left|\tilde{J}\right|_2 \int_0^1 \left(\int_{\frac{a}{a-\tilde{\eta}_2}}^1 \left(f\tilde{\xi}_2\right) \mathrm{d}\tilde{\xi}_2 \right) \mathrm{d}\tilde{\eta}_2 + \left|\tilde{J}\right|_3 \int_0^1 \left(\int_{\frac{a}{a+\tilde{\eta}_2-1}}^1 \left(f\tilde{\xi}_3\right) \mathrm{d}\tilde{\xi}_3 \right) \mathrm{d}\tilde{\eta}_3 & \text{for} \quad a < 0 \\ \left|\tilde{J}\right|_1 \int_0^1 \left(\int_{\frac{a+b-1}{a+b+\tilde{\eta}_1-1}}^1 \left(f\tilde{\xi}_1\right) \mathrm{d}\tilde{\xi}_1 \right) \mathrm{d}\tilde{\eta}_1 + \left|\tilde{J}\right|_2 \int_0^1 \left(\int_{\frac{a+b-1}{a+b-\tilde{\eta}_2}}^1 \left(f\tilde{\xi}_2\right) \mathrm{d}\tilde{\xi}_2 \right) \mathrm{d}\tilde{\eta}_2 & \text{for} \quad a,b \geq 0. \end{cases} \tag{11}$$

Up to three cases are given in the first and third rows of the expressions on the right-hand side: $a < 0$ or $a = 0$ or $a > 0$ for $b < 0$ as well as $(a = 0, b > 0)$ or $a, b > 0$ or $(a > 0, b = 0)$ for $a, b \geq 0$. One or two cases are comprised in the second row: $b = 0$ or $b > 0$ for $a < 0$. Depending on $\left|\tilde{J}\right|_l$, as given in eqns (2)-(4), some integrals may be void or negative. The integration limit $\tilde{\xi}_l \to 0$ is never reached.

3.1 Evaluation of the diagonal terms of the double-layer potential matrix

The evaluation of the block diagonal terms of matrix $\mathbf{H}$ involves in general the finite-part evaluation of singular integrals – after an adequate interval normalization procedure – plus the addition of a discontinuous term. Although a simple task for 2D problems [2], this may become computationally complicated and a source of numerical inaccuracies for 3D problems. In the present framework of integrals evaluated analytically for flat elements, however, we just create for a given source point s, such as node 3 in the illustration on the left in Fig. 2, which is shared by five elements, a fictitious node (here indicated as 7) and evaluate analytically the terms H_{3n} for this small subdomain, with non-void results, according to eq. (8), only for the elements that share the fictitious node. Moreover, if we choose this fictitious node to coincide with any of the nodes depicted as 1 through 6 in the illustration, two of the created triangles turn out to be void, which simplifies evaluations. After that, the diagonal term H_{33} of the actual problem in the illustration is accurately evaluated by requiring that $\sum_i^7 H_{3i} = 0$. The possibility of a local concavity is duly accounted for by just setting, for a general source point s, $H_{ss} \leftarrow \mathrm{frac}(1 + H_{ss})$, where "frac()" is the fractional part of a number.

[1] Maple 15. Maplesoft, a division of Waterloo Maple Inc., Waterloo, Ontario.

4 A simple numerical illustration

4.1 Problem description

Figure 2 represents on the right a very irregular 3D domain with a cavity (drawing rotated with angles $\vartheta = 105^0$, $\varphi = 80^0$), whose boundary is discretized with 16 linear triangle elements and 12 nodes. This is a development of the numerical example presented in [3]. The Cartesian coordinates of these nodes are

$$Coord = \left[\begin{array}{cccccccc} 1 & 2 & 3 & 4 & 5 & 6 & 7 & 8 \\ \hline 1 & 1 & 0.2 & -1 & -2 & -1 & 0.5 & -0.25 \\ -0.5 & 0.4 & 0 & 0.5 & 0 & -0.5 & -1 & -0.55/3 \\ 0.5 & -0.5 & 1 & 1 & -0.2 & 0.5 & -1 & 0.05 \end{array}\right.$$

$$\left.\begin{array}{cccc|cc|cc|cc} 9 & 10 & 11 & 12 & \tilde{1} & \tilde{2} & \tilde{3} & \tilde{4} & \tilde{5} & \tilde{6} \\ \hline -0.3 & -0.5 & -0.4 & 0 & -0.035 & 0.285 & -0.075 & 0.16 & 1.04 & -0.3 \\ -0.2 & -0.1 & -0.3 & 0 & -0.275/3 & -0.5 & -0.605/3 & -0.02 & 0.42 & -0.15 \\ 0.3 & 0.4 & 0.5 & 0.6 & 0.475 & -0.05 & 1.055 & 1.075 & -0.575 & 0.45 \end{array}\right], \tag{12}$$

using the first row for the node numbering, in an array that also contains the coordinates of internal points $\tilde{1}, \tilde{2}$ and external points $\tilde{3}, \tilde{4}, \tilde{5}, \tilde{6}$ at which potential and flow results are to be evaluated. The nodal incidence is

$$Inc = \left[\begin{array}{cccccccccccc|cccc} 1 & 2 & 3 & 4 & 5 & 6 & 7 & 8 & 9 & 10 & 11 & 12 & 13 & 14 & 15 & 16 \\ \hline 1 & 3 & 5 & 5 & 3 & 1 & 8 & 4 & 4 & 8 & 7 & 7 & 9 & 10 & 9 & 9 \\ 2 & 2 & 3 & 6 & 6 & 3 & 2 & 2 & 8 & 6 & 6 & 8 & 10 & 12 & 11 & 12 \\ 3 & 4 & 4 & 3 & 7 & 7 & 1 & 8 & 5 & 5 & 8 & 1 & 11 & 11 & 12 & 10 \end{array}\right]. \tag{13}$$

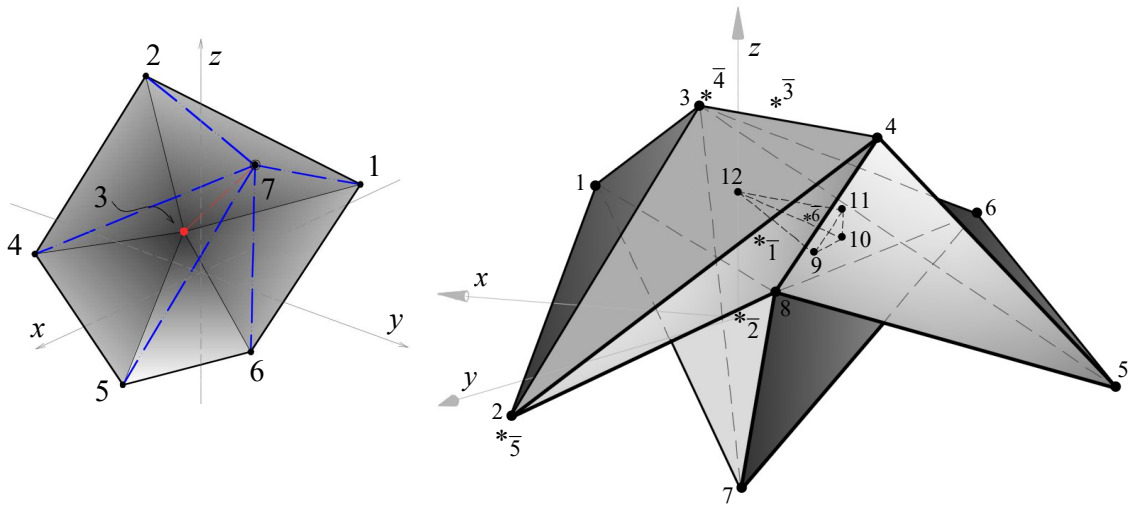

Figure 2. Left: illustration of the scheme for the evaluation of the diagonal terms of **H** referred to node 3 by creating a fictitious node 7 and working with the shown local subdomain; right: very irregular domain with internal points $\tilde{1}, \tilde{2}$ and external points $\tilde{3}, \tilde{4}, \tilde{5}, \tilde{6}$ at which potential and flow results are to be evaluated

It is worth observing that elements 6 (nodes [1 3 7]) and 12 (nodes [7 8 1]) are almost coplanar. Nodes 9-12 correspond to a cavity built up with elements 13-16 (node 10 is closer to the observer than nodes 9 and 11). The external point $\tilde{6}$ is in the center of the cavity. All nodes and internal and external points are very close to the boundary segments. Consistency check of the boundary element equation **Gt = Hd** for 3 linearly varying

potential fields holds for 19 digits in a Maple implementation with 20 digits of computation precision. The internal point $\tilde{1}$ and the external points $\tilde{3}, \tilde{6}$ present complex quasi-singularities with respect to all 16 elements, with flow evaluated according to eqn (9). The internal point $\tilde{2}$ is on the plane of element 6 and the corresponding flow must be evaluated in terms of all three sub-triangles as given in the second row on the right-hand-side of eqn (11), for $a = -0.1$, $b = 0.55$, with negative area for sub-triangle 1. The external points $\tilde{4}$ and $\tilde{5}$ are in the intersection of the planes given by elements 1 and 2. Flow results at point $\tilde{4}$ require evaluations for element 1 ($a = 0$, $b = -0.05$) over sub-triangles 2 (negative area) and 3, and for element 2 ($a = 1.05$, $b = -0.05$) over sub-triangles 1 and 2 (the latter with negative area), both cases according to the first row of eqn (11). Flow results at point $\tilde{5}$ require evaluations for element 1 ($a = 0$, $b = 1.05$) over sub-triangles 2 and 3 (negative area) according to the third row of eqn (11), and for element 2 ($a = -0.05$, $b = 1.05$) over sub-triangles 1 (negative area) and 2 according to the second row of eqn (11). Then, all possible cases of quasi-singularity and topology issues are numerically assessed.

For 3 linearly varying potential fields, accuracy of potential results at all six points is checked for about 18 digits. For flow results round-off errors unavoidably occur and accuracy is checked for at least 16 digits in the case of points $\tilde{1}, \tilde{2}, \tilde{6}$ and at least 13, 12 and 10 digits in the case of points $\tilde{3}$, $\tilde{4}$ and $\tilde{5}$, respectively (results at external points $\tilde{3}, \tilde{4}, \tilde{5}, \tilde{6}$ obviously compare to zero). These internal point assessments are summarized in Table 1.

Table 1. Summary of the results at internal points for the solid on the right in Fig. 2 submitted to 3 linear potential fields – the operations with $\Delta_1 \ldots \Delta_3$ refer to eqns (10) and (11)

Point	Type	Planar to element	(a, b)	$\iint$	Potential accuracy	Flow accuracy
$\tilde{1}$	Internal	–	–	eqn (9)	18 digits	16 digits
$\tilde{2}$	Internal	$6 \to [1,3,7]$	$(-0.1, 0.55)$	$-\Delta_1 + \Delta_2 + \Delta_3$	18 digits	16 digits
$\tilde{3}$	External	–	–	eqn (9)	18 digits	13 digits
$\tilde{4}$	External	$1 \to [1,2,3]$ $2 \to [3,2,4]$	$(0, -0.05)$ $(1.05, -0.05)$	$-\Delta_2 + \Delta_3$ $\Delta_1 - \Delta_2$	18 digits	12 digits
$\tilde{5}$	External	$1 \to [1,2,3]$ $2 \to [3,2,4]$	$(0, 1.05)$ $(-0.05, 1.05)$	$\Delta_2 - \Delta_3$ $-\Delta_1 + \Delta_2$	18 digits	10 digits
$\tilde{6}$	External (cavity)	–	–	eqn (9)	18 digits	16 digits

5 On the use of adaptive numerical quadrature

The literature on numerical quadrature schemes for 3D boundary element problems is vast and shall not be explored here. In spite of recent attempts to develop efficient quadrature schemes for triangle elements, the proposition by Dunavant [6] over three decades ago from developments started by Hammer et al [7] as early as in the year 1956 seems unbeatable, as abscissas and weights are evaluated directly in triangle coordinates so that the Jacobian of coordinate transformation is constant and does not add to an integrand's complexity. Dunavant presents in his paper a large table of abscissas and weights for the accurate evaluation of complete bivariate polynomials of degrees 1 through 20 with 15 digits of precision. This scheme has been implemented in the present paper in order to evolve from analytical to adaptive numerical quadrature with complete error control. (We have already evolved further to a fast multipole implementation for the case of source point and boundary element very far from each other – always with complete error control, as presented in a companion contribution to this conference.)

Figure 3 singles out on the right the triangle element $\#1$ of the example above, according to the node incidence of eq. (13) and the coordinates given in eq. (12). From the middle coordinate point $C_0 = [2.2, -0.1, 1.]/3$ of the triangle's nodes we draw a sequence of seven points along a horizontal line, $s_i = C_0 + [1, 0, 0].10^i, i = -3 \ldots 3$, at which we evaluate potential and gradient results for three linear potential fields $[x, y, z]$ independently applied to the open domain and measured as potentials and gradients on the element surface. The vector of values in the figure displays the relative distances from these points to the triangle's surface given as $\Delta r_i/\sqrt{A}, i = 1 \ldots 7$, where Δr_i corresponds to $\overline{OP}$ on the left in Fig.1 and A is the triangle's area. The Frobenius norms of potential and gradient results for the three independent fields are then evaluated numerically, according to Dunavant's scheme, for the seven "internal" points and compared with the target, analytical results obtained according to the previous Sections. Since the applied potential fields are linear, the analytical results are accurate within machine precision (20 digits, as implemented) and taking into account unavoidable roun-off errors, as shown in the previous Section.

The accuracy assessment of the quadrature results for just one triangle is justified as we have in the evaluation for a complete problem with a large number of elements the eventual occurrence of large errors affecting integrals of small magnitudes – with no sensible conclusion to be drawn.

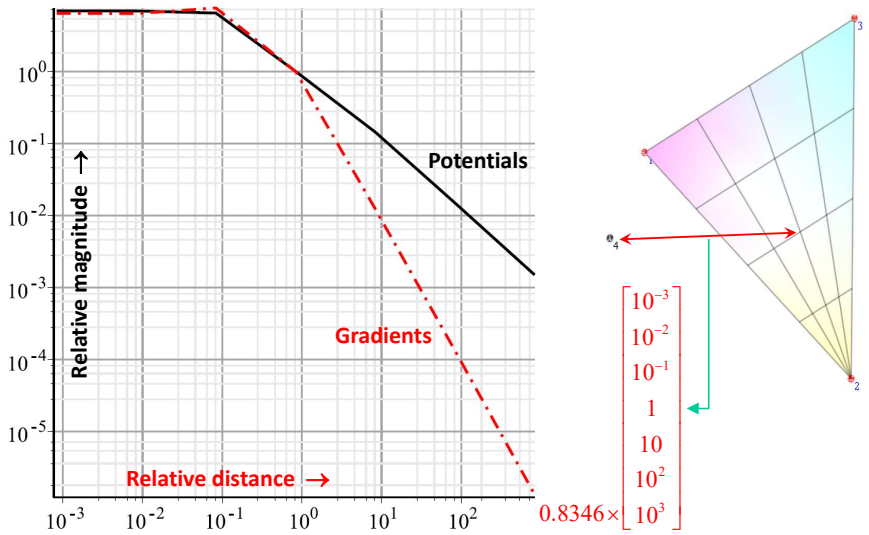

Figure 3. Contribution of boundary data on the indicated triangle for the relative potential and gradient magnitude results at seven internal points located at the indicated relative distances

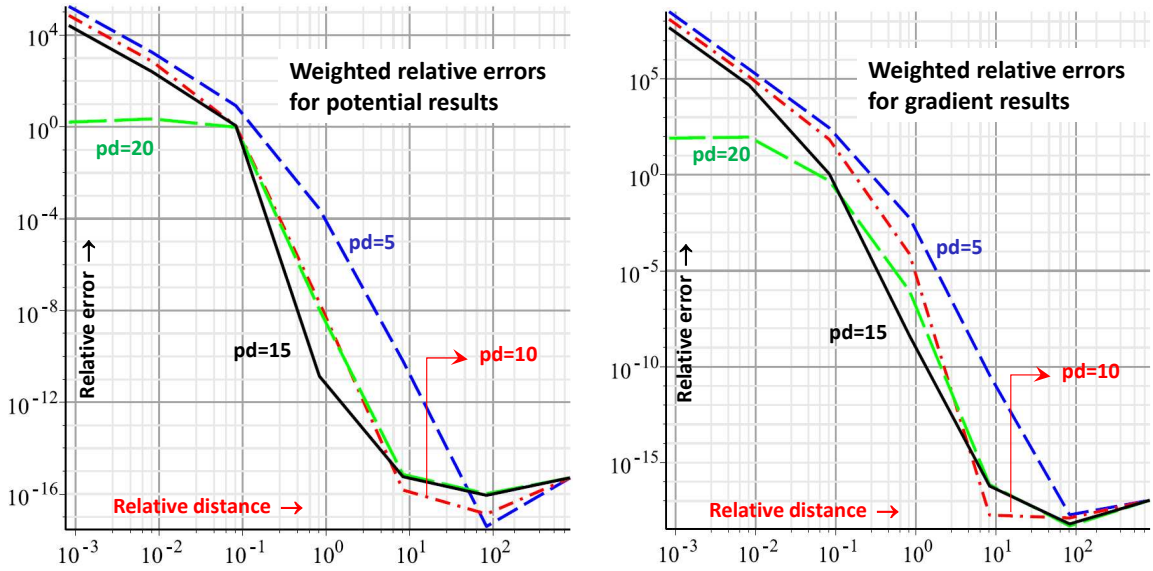

Figure 4. Relative potential and gradient quadrature (accuracy for polynomial degrees 5, 10, 15 and 20) error results at the seven indicated internal points of Fig. 3 weighted with respect to the results at point $\#4$

This seven distinct relative distances are given as the abscissas of the double logarithmic graph in Fig. 3, with the ordinate displaying analytically evaluated potential and gradient Frobenius norms divided by the corresponding values for point $\#4$ – the only one that could be pictured, as shown on the right. The integral values for points very close to the triangle are up to ten times the values for point $\#4$ and decrease considerably as the points become more distant, and this particularly for the gradients. With this knowledge we are now able to properly assess the practical accuracy of Dunavant's quadrature scheme by constructing the same Frobenius norms just introduced for the analytical evaluations. Figure 4 shows weighted relative errors of the numerically evaluated potential and gradient results at the seven "internal" points, obtained according to the formula $error = (num_i - anal_i)/anal_4$, $i = 1 \ldots 7$, that is, weighted by the results for point $\#4$ in order to include the relative magnitudes made evident in the graph of Fig. 3. The quadratures are for Dunavant's schemes accurate for complete bivariate polynomials of degrees pd = 5, 10, 15 and 20. We see that for relative distances much smaller than 1 a numerical quadrature

leads to absurd results, for relative distances from about 1 to 10 conditionally good results are achievable in terms of some adaptive scheme, whereas for relative distances larger than 10 a very low order quadrature scheme does the job satisfactorily. On the other hand, this already enters the realm of the fast multipole method!

6 Conclusions

The analytical developments of this paper for steady-state potential problems and using the T3 element apply to elastostatics problems and flat Q4 elements, as well, requiring only some additional effort in the code implementation. A rather academical, but topologically challenging, example attests to the accuracy that is achievable within machine precision and having round-off errors into account. We also assess the circumstances of combining analytical evaluations for source point and boundary element close to each other – which includes evaluations at internal points – with an adaptive numerical quadrature as the distances increase, in a way that enables complete control of result's precision. We already have an implementation that includes in the evolution from analytical evaluations to adaptive numerical quadrature a fast multipole scheme for the simulation of problems with a very large number of degrees of freedom.

Acknowledgements. This project was supported by the Brazilian agencies CAPES and CNPq.

Authorship statement. The authors hereby confirm that they are the sole liable persons responsible for the authorship of this work, and that all material of the present paper is the property (and authorship) of the authors.

References

[1] C. A. Brebbia, J. C. F.Telles, and L. C. Wrobel. *Boundary Element Techniques*. Springer-Verlag, 1984.
[2] N. A. Dumont. The collocation boundary element method revisited: Perfect code for 2D problems. *International Journal of Computational Methods and Experimental Measurements*, vol. 6, n. 6, pp. 965–975, 2018.
[3] N. Dumont and T. G. Kurz. Analytical 3D boundary element implementation of flat triangle and quadrilateral elements for potential and linear elasticity problems. In A. H.-D. Cheng and A. Tadeu, eds, *Boundary Elements and other Mesh Reduction Methods XLII*, volume 26 of *WIT Transactions on Engineering Sciences*, pp. 1–11. WIT Press, 2019.
[4] T. G. Kurz. *Analytical evaluation of the integrals of flat boundary elements for three-dimensional potential and elasticity problems*. PhD thesis, Pontifícia Universidade Católica do Rio de Janeiro. (In Portuguese), 2021.
[5] J. C. Lachat and J. O. Watson. Effective numerical treatment of boundary integral equations: A formulation for three-dimensional elastostatics. *International Journal for Numerical Methods in Engineerings*, vol. 10, n. 5, pp. 991–1005, 1976.
[6] D. A. Dunavant. High degree efficient symmetrical Gaussian quadrature rules for the triangle. *International Journal for Numerical Methods in Engineering*, vol. 21, pp. 1129–1148, 1985.
[7] P. C. Hammer, O. J. Marlowe, and A. H. Stroud. Numerical integration over simplexes and cones. *International Journal for Numerical Methods in Engineering*, vol. 10, pp. 130–137, 1956.